Fluorescent styrylpyrylium probes for the imaging of mitochondria in live cells

Ignacio Muñoz Resta,[†] Federico Lucantoni,[‡,§] Nadezda Apostolova,[*,‡,§,#] Francisco Galindo[*,†]

†. Departamento de Química Inorgánica y Orgánica, Universitat Jaume I, Av. V. Sos Baynat s/n, 12071, Castellón, Spain. E-mail: francisco.galindo@uji.es

‡. Departamento de Farmacología, Facultad de Medicina, Universidad de Valencia, Av. Blasco Ibañez n. 15-17, 46010, Valencia, Spain. E-mail: nadezda.apostolova@uv.es

§. FISABIO (Fundación para el Fomento de la Investigación Sanitaria y Biomédica de la Comunitat Valenciana), Spain.

#. CIBERehd (Centro de Investigación Biomédica en Red: Enfermedades hepáticas y digestivas), Spain.

Abstract: Eight styrylpyrylium tetrafluoroborate salts have been synthesized and fully optically characterized by UV-vis absorption and fluorescence steady-state / time-resolved spectroscopies. The new dyes display strong emission bands with yellow-orange colours, depending on the substituents present in the structure. Notably, the Stokes shift recorded for some of them exceeds 100 nm, a very valuable feature for biological imaging. Four of them have been assayed as biological imaging agents by confocal laser scanning microscopy (CLSM) in the human hepatoma cell line Hep3B. It has been found that all the compounds stain efficiently intracellular structures which have been identified as mitochondria through colocalization assays with MitoView (a well-known mitochondrial marker) and by using carbonyl cyanide m-chlorophenyl hydrazone (CCCP) as mitochondrial membrane potential uncoupler. Additionally, the potential ability of the studied dyes as cytotoxic drugs has been explored. Inhibitory concentration (IC_{50}) against Hep3B was found to be in the range of 4.2 μM - 11.5 μM, similar to other described anticancer drugs for the same hepatoma cell line. The combined features of a good imaging agent and potential anticancer drug make the family of studied pyrylium salts good candidates for further theranostic studies. Remarkably, despite the extensive use of pyrylium dyes in several scientific areas (from photocatalysis to optics), there is no precedent description of a styrylpyrylium salt with potential theranostic applications.

Introduction

Mitochondria are one of the most versatile cellular organelles because they are involved in multiple biologically relevant processes taking place in eukaryotic organisms. Commonly known as *powerhouses of the cell*, their functions vary from energy production to important roles in metabolism, innate immunity, and intrinsic apoptosis, just to mention a few.[1] Morphologically, mitochondria are the only organelles in animal cells with two membranes: an outer one, porous and permeable, and an inner one with very restricted transport properties.[2] Is onto this latter one, and in the isolated space that it encircles, the mitochondrial matrix, that the key function of mitochondria takes place: oxidative phosphorylation. This metabolic process couples the energy released from a series of redox reactions to the translocation of protons from the matrix to the external side of the inner membrane, thus generating a proton gradient that acts as the driving force for the synthesis of ATP, the universal intermediate that serves as the energy source for most of the chemical reactions that occur within the cells.[3]

Because of the highly negative potential that is generated due to the proton flux through the inner membrane, delocalized lipophilic cations, DLCs, accumulate efficiently within mitochondria.[1,4] This class of molecules are species with a positive charge and a π-conjugated system, with the possibility of fine-tuning the charge distribution and polarity by the introduction of different substituents.[5] As fluorescence microscopy is a well-established technique for cell imaging, a great number of reported emissive DLCs has expanded the library of small-molecule fluorescent probes for visualizing mitochondria.[1,2,4,6–9]

Some examples of DLCs as mitochondrial fluorescent markers comprise molecules as diverse as rhodamines,[10–12] bisamidines,[13,14] coumarin-based fluorophores,[15–19] indole-

ring substituted derivates,[5] pentamethinium salts,[20] quaternized imidazole [1,2-a]-pyridines[21], boron dipyrromethenes (BODIPYs)[22], tetraphenylethylene derivates[23,24] and, cyanine dyes.[25,26] Notably, exceptions are described and certain probes targeting mitochondria are neutral compounds, such as the recently developed acridone derivates, described by the group of A. Orte.[27] An innovative novel approach for the generation of mitochondrial markers utilizes a completely different mechanism, mediated by the enzyme carnitine-acylcarnitine translocase (CACT) to deliver the probe inside the organelle (regardless of the transmembrane potential).[28] However, one common limitation of most reported mitochondrial probes based on xanthenic, cyanine and BODIPY architectures is their small Stokes shift (SS). For instance, the SS of paradigmatic examples of mitochondrial probes like rhodamine 123, tetramethyl rhodamine methyl ester (TMRM) and DiOC6(3) is scarcely a few nanometers.

Alterations in mitochondrial physiology are associated with a vast number of human conditions such as neurological, cardiovascular, metabolic, and neoplastic diseases. It is well known that DLCs can be toxic to the organelle at high concentrations.[3] So, besides acting as fluorescent markers, they could also be used as therapeutic agents in the treatment of mitochondrial disorders.[29,30] Although all DLCs share the same mechanism for accumulation in the mitochondria, i.e., response to negative inside transmembrane potential, their mechanisms of toxicity are relatively diverse and points to different targets, such as the electron transport chain, the mitochondrial permeability or specific enzymes of the organelle.[31]

Pyrylium dyes comprise a well-characterized family of compounds with a large variety of applications in fields as varied as photocatalysis,[32–35] photodynamic therapy (PDT),[36] chemosensing,[37,38] organic synthesis,[39] optics,[40] etc., but the number of pyrylium

dyes designed to image living cells is scarcer.[41,42] Although the number of chemical families used for mitochondrial staining is high (see above), pyrylium dyes have been reported only in few cases during the last years for that purpose.[41,42,43–45] Additionally, although not used for bioimaging, several pyrylium salts have been studied as potential anticancer drugs[46,47] pointing to mitochondria as the site of action.

One important advantage of pyrylium dyes over other chemical families is their easy synthesis and purification,[48] in addition to high emission quantum yields,[49] which make them very attractive for bioimaging applications. Another benefit of pyrylium dyes is that they do not tend to participate in type I or II photosensitization processes, thus preventing photodamage during image acquisition by generated reactive oxygen species (ROS). Here we report the synthesis and characterization of eight styrylpyrylium dyes (**Chart 1**). Four of them have been tested and found useful for mitochondrial fluorescence bioimaging in cultured hepatocarcinoma cells (Hep3B). Notably, the described pyrylium dyes display large SS depending on the substitution and the solvent (more than 100 nm in some cases). We believe that these probes can be added to the current arsenal available for the imaging of living cells[50–52] and, eventually, be evaluated as mitochondrial drugs.

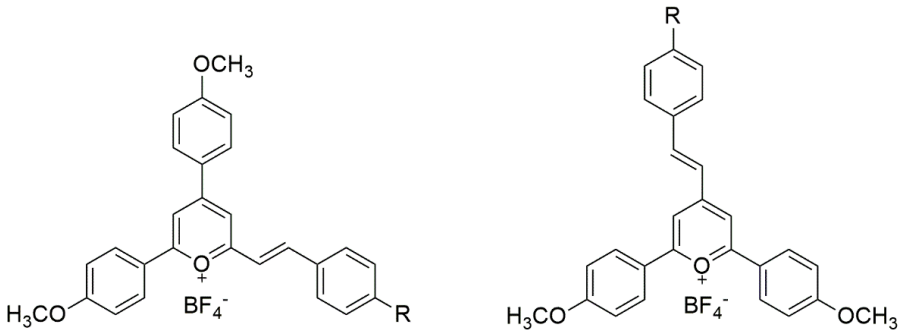

1a R = -H
1b R = -CF_3
1c R = -OH
1d R = -OCH_3

2a R = -H
2b R = -CF_3
2c R = -OH
2d R = -OCH_3

Chart 1. Styrylpyrylium dyes synthesized and studied in the present work.

Results and discussion

Synthesis and characterisation

Following procedures used previously for the preparation of similar compounds in our group,[40,53] dyes **1a-d** were prepared in a two-step process as shown in **Scheme 1**. A condensation between *p*-metoxyacetophenone and acetic anhydride catalysed by BF_3-etherate led to the intermediate 2,4-bis(4-methoxyphenyl)-6-methylpyrylium tetrafluoroborate. The reaction between this intermediate and the corresponding *p*-substituted benzaldehydes in acetic acid resulted in the desired products, all of them easily purified by precipitation in diethyl ether and obtained in moderate to high yields (74 – 87%).

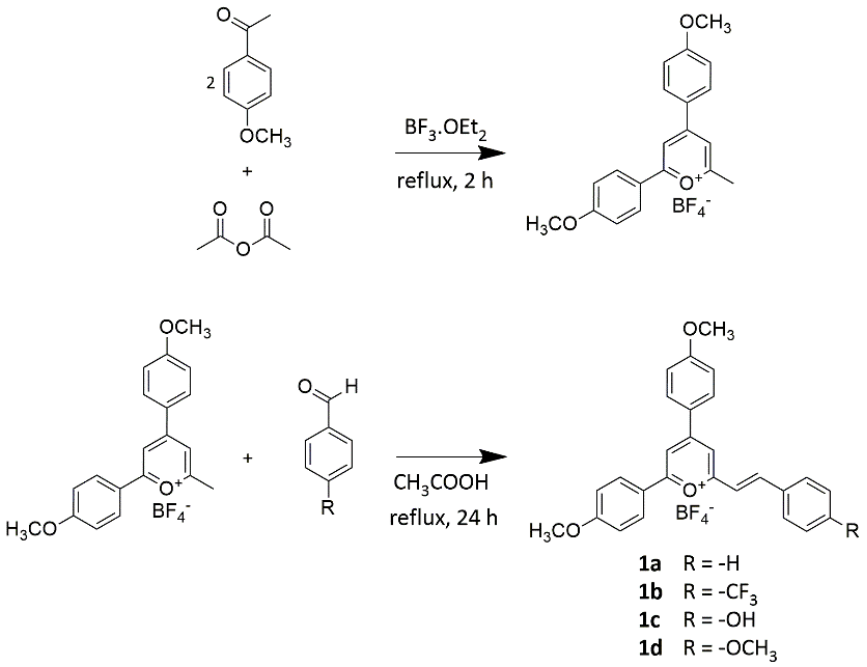

Scheme 1. Synthesis of compounds **1a-d**.

A related family of compounds with the same substituents but a different position of the styryl chain were synthesized, as can be seen in **Scheme 2**, adapting a previously reported procedure.[54] The synthesis of the intermediate 2,6-bis(4-methoxyphenyl)-4-methylpyrylium

tetrafluoroborate was carried out in three consecutive steps, following by the reaction with the corresponding *p*-substituted benzaldehydes to yield the required products **2a-d**. The obtained compounds were isolated simply by precipitation in diethyl ether (yields 58-86 %), avoiding chromatographic techniques, thus providing a comparative advantage over other probes.

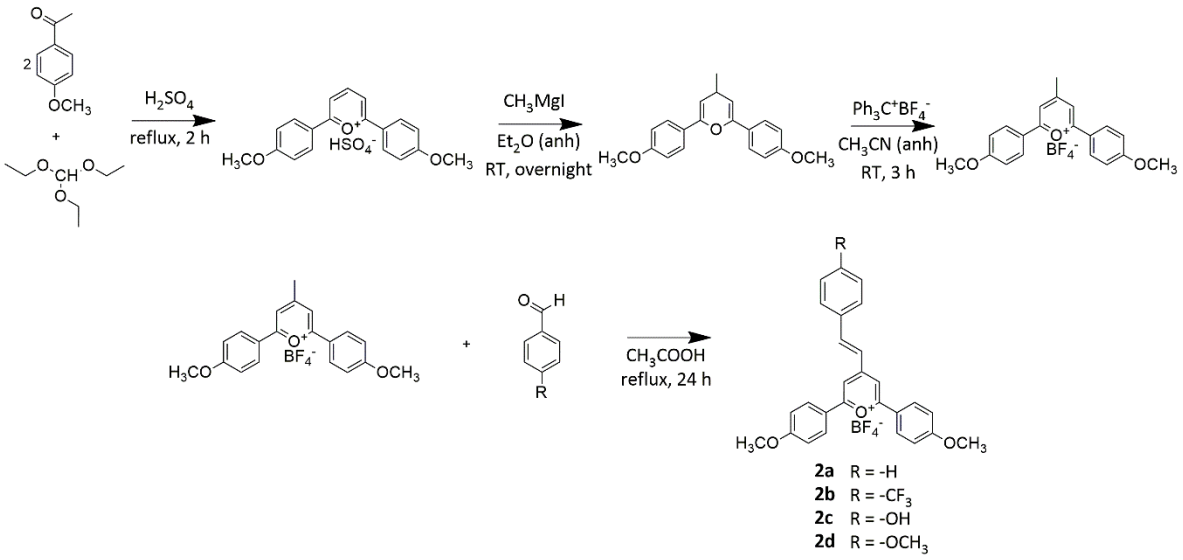

Scheme 2. Synthesis of compounds **2a-d**.

All eight compounds are strongly coloured, with emissions within the yellow and the orange (**Figures 1-4**). Their photophysical properties were determined in three solvents of different polarities: dichloromethane (DCM), acetonitrile (ACN), and phosphate-buffered saline (PBS) 10 mM, pH 7.4. The data for all the compounds are collected in **Table 1**.

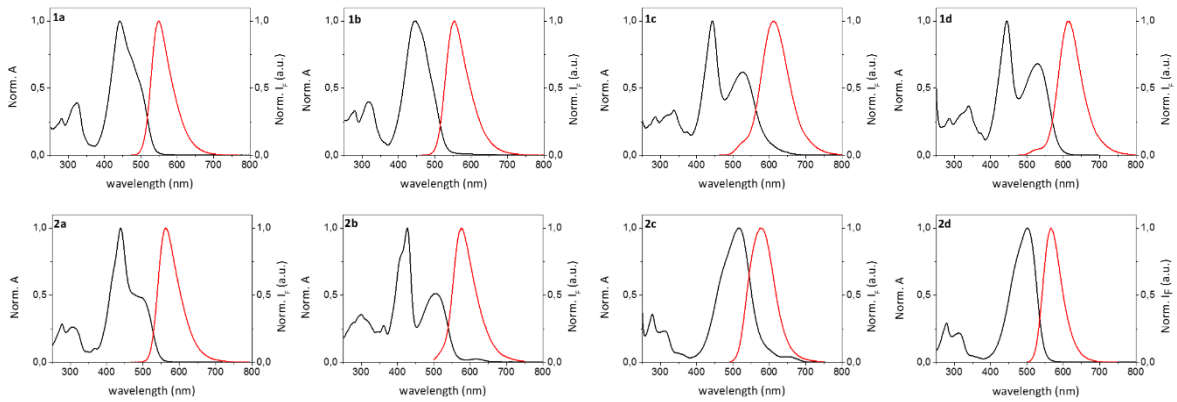

Figure 1. Normalized absorption (black) and emission (red) spectra of compounds **1a-d, 2a-d** in DCM. λ_{exc} was set at the absorption maximum of each compound.

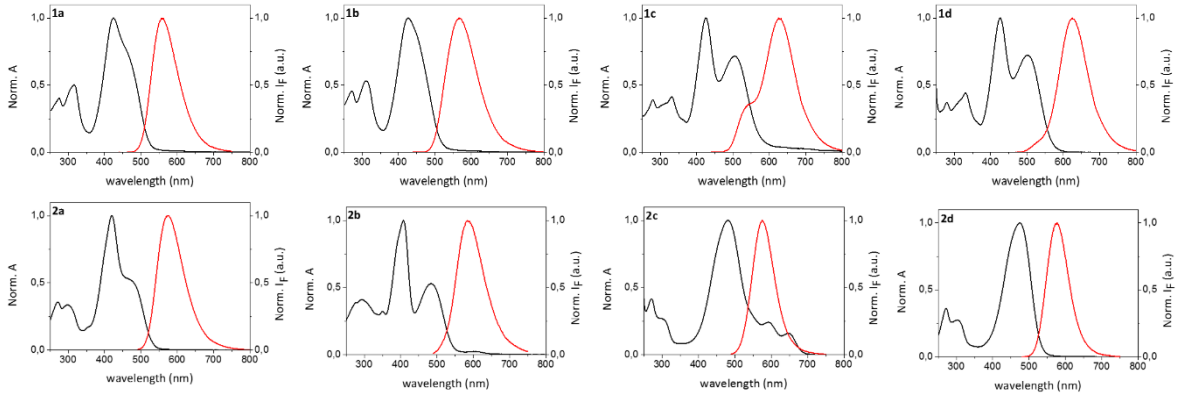

Figure 2. Normalized absorption (black) and emission (red) spectra of compounds **1a-d**, **2a-d** in ACN. λ_{exc} was set at the absorption maximum of each compound.

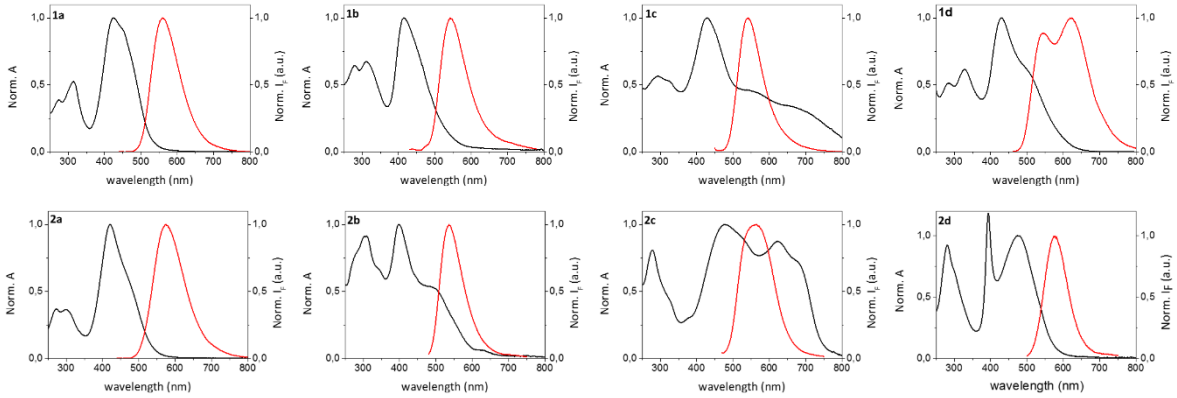

Figure 3. Normalized absorption (black) and emission (red) spectra of compounds **1a-d**, **2a-d** in PBS (10 mM, pH 7.4). λ_{exc} was set at the absorption maximum of each compound.

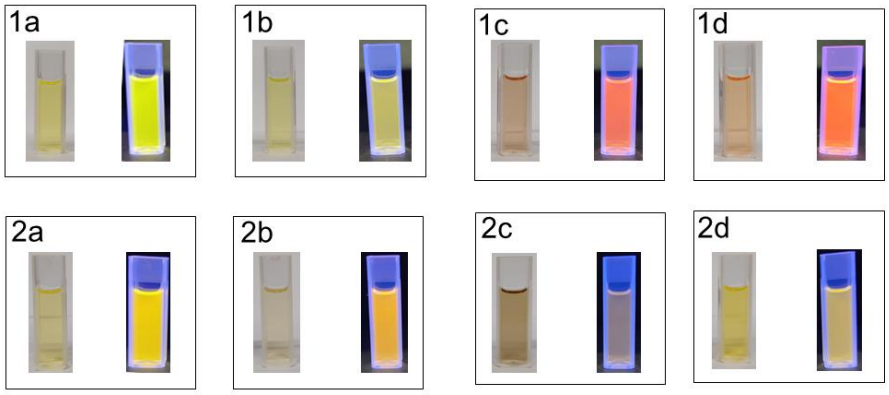

Figure 4. 10 uM solutions of compounds **1a-d**, **2a-d** in acetonitrile under visible (left) and UV -365 nm- (right) light.

Table 1. Photophysical parameters for different solutions of compounds **1a-d** and **2a-d**.

Compd.	Sv.	λ_{abs} (log ε) (nm)	λ_{em} (nm)	ϕ_F	τ_F (ns)
1a	ACN	424 (4.64)	557	0.49	$\tau_1 \leq 1.0$ (11 %) $\tau_2 = 3.5$ (89 %)
	DCM	442 (4.75)	548	0.95	4.6
	PBS 10 mM pH = 7.4	425 (4.53)	561	0.10	$\tau_1 \leq 1.0$ (82%) $\tau_2 = 3.4$ (18 %)
1b	ACN	426 (4.57)	568	0.13	$\tau_1 = 1.1$ (75 %) $\tau_2 = 5.2$ (25 %)
	DCM	446 (4.67)	553	0.72	4.7
	PBS 10 mM pH = 7.4	415 (4.30)	542	0.01	$\tau_1 \leq 1.0$ (25 %) $\tau_2 = 3.8$ (75 %)
1c	ACN	425 (4.63) 504 (4.49)	535 -s- 625	0.17	$\tau_1 \leq 1.0$ (43 %) $\tau_2 = 2.2$ (57 %)
	DCM	443 (4.71) 527 (4.50)	505 -s- 613	0.38	$\tau_1 = 1.1$ (15 %) $\tau_2 = 3.2$ (85 %)
	PBS 10 mM pH = 7.4	427 (4.37)	541	0.01	$\tau_1 \leq 1.0$ (9 %) $\tau_2 = 3.7$ (91 %)
1d	ACN	426 (4.66) 501 (4.49)	625	0.38	$\tau_1 \leq 1.0$ (8 %) $\tau_2 = 3.5$ (92 %)
	DCM	445 (4.77) 529 (4.60)	525 614	0.59	4.0
	PBS 10 mM pH = 7.4	430 (4.43) 500 -s-	546 623	0.03	$\tau_1 \leq 1.0$ (83 %) $\tau_2 = 3.3$ (17 %)
2a	ACN	420 (4.65) 475 -s-	575	0.39	3.6
	DCM	439 (4.78) 490 -s-	562	0.61	4.1
	PBS 10 mM pH = 7.4	421 (4.54)	573	0.06	$\tau_1 \leq 1.0$ (87 %) $\tau_2 = 3.5$ (13 %)
2b	ACN	408 (4.61) 483 (4.33)	584	0.22	2.1
	DCM	427 (4.68) 504 (4.39)	575	0.45	4.2
	PBS 10 mM pH = 7.4	398 (4.38) 500 -s-	536	0.005	$\tau_1 \leq 1.0$ (46 %) $\tau_2 = 4.0$ (54 %)
2c	ACN	481 (4.72) 593 (4.10) 647 (3.92)	576	0.09	≤ 1.0
	DCM	517 (4.82) 653 (3.46)	577	0.37	1.3
	PBS 10 mM pH = 7.4	478 (4.33) 621 (4.27) 680 -s-	566	0.007	$\tau_1 \leq 1.0$ (89 %) $\tau_2 = 3.8$ (11%)
2d	ACN	474 (4.77)	578	0.28	≤ 1.0
	DCM	501 (4.87)	567	0.54	1.2
	PBS 10 mM pH = 7.4	474 (4.25)	577	0.01	≤ 1.0

s = shoulder

The pyrylium salts here studied show one or two intense absorption bands above 400 nm (see spectra in **Figures 1-3** and data in **Table 1**). According to the literature, pyrylium dyes can be considered as two-dimensional chromophoric systems displaying X and Y absorption bands.[49] In the case of styrylpyrylium salts characterized in this study and

according to previous works,[55,56] the electronic transition that originates the band at shorter wavelengths (chromophore Y, around 400 nm) can be assumed to be strongly localized on the pyrylium core and, on the other hand, the transition with the lowest energy (chromophore X, around 450-500 nm) can be associated to the whole conjugated system. Sometimes, depending on the solvent, but particularly on the substitution pattern, these two bands overlap and only one transition can be seen. The case of compounds **1c** and **2c** is special since, in PBS, the absorption spectra are extended towards very low energies, beyond 700 nm. This behaviour in PBS can be ascribed to the formation of a new band due to the acid-base equilibrium established between the pyrylium cation and the quinoidal base formed after deprotonation of the free OH (**Figure S16** in the Supplementary Data File). Related compounds, like flavylium salts, have also shown this acid-base behaviour.[57] And recently, a pyrylium dye with hydroxyl groups has been reported to show a similar shift in the absorption spectrum, from 460 nm to 570 nm, upon deprotonation.[41] Regarding the fluorescence properties of the studied dyes, mainly one emission band is observed, except for particular situations like compound **1d** in PBS and compound **1c** in ACN, which show dual fluorescence (very clear for **1d** and in the form of a shoulder for **1c**). Nikolov and Vauthey have demonstrated that related compounds (6-styryl-substituted-2,4-diphenyl pyrylium cations) display *non-Kasha* fluorescence behaviour, with two emission bands, one localized in the pyrylium core (L band) and other delocalized throughout the whole dye (D band). Besides, those L and D bands do not exhibit a precursor-successor relationship.[55,56] In the set of molecules here studied, such double fluorescence is not a common pattern, but, as mentioned early, an exception. Likely, the D band (S_2-S_0 transition) is not observable for most of the molecules, but only the lower S_1-S_0 one. Probably, the fact that aryl rings in positions 2 and 4 are substituted with a methoxy substituent implies the formation of a less

stabilized charge-transfer (CT) state than for the compounds studied by Nikolov and Vauthey, lacking such methoxy substituent. As a matter of fact, the early reported dyes displayed D emissions more bathochromically shifted (up to 630 - 645 nm depending on the solvent) than any of the studied here. Although it would be desirable to have dual emission features in systems aimed for biological imaging, in the case of the pyrylium dyes aqueous stability is a matter of the utmost importance, and the presence of methoxy groups is mandatory to avoid aqueous hydrolysis, since the donating MeO- groups stabilize the central pyrylium core, thus hampering the opening of the central ring (and loss of colour and emission).[44] Finally, regarding the fluorescence quantum yields, it must be noted that higher values have been recorded in nonpolar dichloromethane than in polar acetonitrile and PBS (**Table 1**). This fact reflects the CT character of the emissive state, in accordance with previous descriptions of analogous styrylpyrylium cations.[49,55,56] Emission lifetimes are complex and cannot be explained by a single model. Likely, as reported earlier,[55] the presence of several conformers could explain the lifetime distributions.

An important feature of molecules **1a-d** and **2a-d** is the large SS observed. This parameter is of great importance to obtain information from biological samples without interference from the excitation source. The absorption and emission spectra of many probes described in the literature, and many of the ones currently commercialized, are separated by scarcely a few nanometers, which causes cross-talk between excitation and fluorescence, implying normally a poor signal-to-noise ratio.[58] The SS of **1a-d** and **2a-d** has been collected in **Table S1** (only in PBS since the biological imaging is the ultimate objective of this work). As it can be seen, the following molecules stand out for their SS, higher than 100 nm (SS value in parenthesis): **1a** (136 nm), **1b** (127nm), **1c** (114 nm), **1d** (193 nm), **2a** (152 nm) and

2d (103 nm). For comparison purposes, common biological fluorescent stains are included in the same table. It must be noted that an approach to achieve larger SS normally described in the literature consists of the combination of two optically active moieties in the same molecule, communicated via Förster Resonance Energy Transfer (FRET) mechanism, or via Excited State Intramolecular Proton Transfer (ESIPT) and extended conjugations.[59,60] However, some of those strategies require a considerable synthetic effort, leading to complex molecules in very low chemical yields. On the contrary, the approach here reported affords notable amounts of dyes in few synthetic steps, and the purification is carried out avoiding chromatographic techniques, only by the precipitation method (typically 200-300 mg of each dye were produced, and the synthesis can be easily escalated).

Cellular imaging

Before carrying out biological assays, a stability test towards hydrolysis over long periods was conducted with all the synthesized compounds. Since pyrylium core is susceptible to nucleophilic attacks due to its electron deficiency, especially at positions 2 and 6, compounds with electron-donating substituents were expected to be more stable to hydrolysis in an aqueous environment. Measurement of the absorbance spectrum of each compound in PBS over time showed that **1a,b** and **2a,b** suffered a fast hydrolytic process making these dyes less suitable for bioimaging assays (data not shown). Hence, live-cell imaging assays were conducted with probes **1c,d** and **2c,d**, more stable than **1a,b** and **2a,b**, (although all showed some tendency to hydrolysis after several hours in PBS). It must be recalled that the search for pyrylium dyes with enhanced aqueous stability is a relevant objective, not only for bioimaging but for other optical applications. In this regard, the group of L. Yuan and L. Shi investigated in detail synthetic strategies to develop rigidized

alkylamino derivatives of pyrylium cations displaying enhanced stability in an aqueous environment.[44]

The cellular uptake and subcellular localization of the four probes were studied by confocal laser scanning microscopy (CLSM) using the human hepatoblastoma cell line Hep3B. The choice of this line is justified both considering that hepatocytes possess many mitochondria compared to other cell types and also regarding the interest of search for drugs with cytotoxic properties in the context of hepatocellular carcinoma (HCC). Visualization of the four dyes within the cells was performed after 30 min of incubation (1 μM of each dye) as shown in **Figure 5A**. Cells were also stained with Hoechst 33342 to mark nuclei. The intensity of the fluorescent signal displayed by **1d** and **2c** was comparable and significantly higher than the intensity displayed by **1c** and **2d**. When cells were exposed to a higher concentration (5 μM) for 30 min, **1d** revealed the highest fluorescence intensity, with saturation of the signal, whereas the rest of the molecules afforded well-resolved images (**Figure 5B**). Thus, since **1d** was the probe rendering the highest fluorescence intensity and cellular internalization, its ability to stain mitochondria was also confirmed with a lower concentration (0.5 μM) as shown in **Figure 5C**. Similar or higher concentrations of pyrylium dyes have been employed for intracellular assays reported in the literature. For instance, 1 μM for dye C2,[43] 5 μM for TPPF-NTF[44] and 20 μM for pentacyclic pyrylium PS-OH.[41]

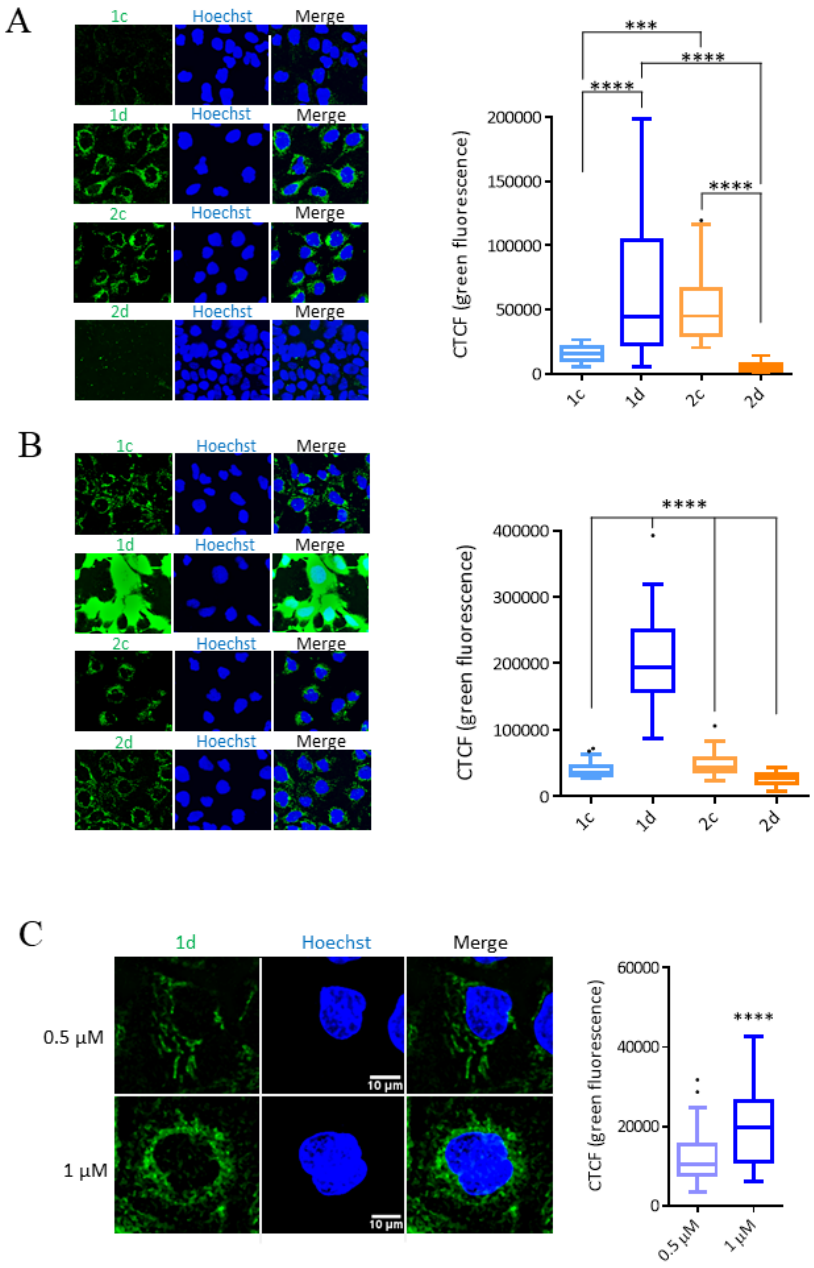

Figure 5. Analysis of the fluorescence intensity by CLSM. Nuclei were stained with Hoechst 33342 (blue) and confocal microscope images were obtained after exposure to (A) 1 µM of **1c**, **1d**, **2c** or **2d**; (B) 5 µM of **1c**, **1d**, **2c** or **2d**; and (C) 0.5 µM or 1 µM of **1d**. Representative images and quantification of the green fluorescent signal (CTCF, corrected total cell fluorescence) are displayed. Data are shown as median ± IQR (inter-quartile range), n=3. Statistical analysis was performed by one-way ANOVA followed by Tukey's multiple comparisons tests (*** indicates a p-value ≤ 0.001 and **** indicates a p-value ≤ 0.0001) for A and B, and unpaired t-test (**** indicates a p-value ≤ 0.0001) for C.

The morphology of the marked subcellular structures, filamentous and interconnected, and their perinuclear location, strongly suggested mitochondrial staining. The pattern of subcellular localization was very similar for the four tested compounds (**Figure 5**). To assess the specificity of the assayed fluorogenic dyes to stain mitochondria, colocalization experiments with the mitochondria-specific far-red fluorescent dye MitoView 633 were performed. To this purpose, pyrylium dyes **1d** (1µM) and **2d** (5µM) were co-incubated with MitoView 633 (100 nM). A clear correlation of each of the fluorochromes with MitoView 633 can be observed in **Figure 6**, indicating the mitochondrial location of the tested compounds, with Pearson´s correlation coefficients of 0.78 and 0.81, respectively. For comparison, correlation analysis was also performed between the fluorescent dyes and the nuclear signal (Hoechst 33348) and as illustrated in **Figure S17**, no colocalization was found. Of note, despite being an excellent mitochondrial marker, MitoView 633 has been reported to have some photosensitization effects, leading to mitophagy, resulting from the generation of reactive oxygen species (ROS), like singlet oxygen ($^1O_2$), upon irradiation.[61] Of note, this process is very unlikely to occur with pyrylium dyes due to their low efficiency generating ROS.[32]

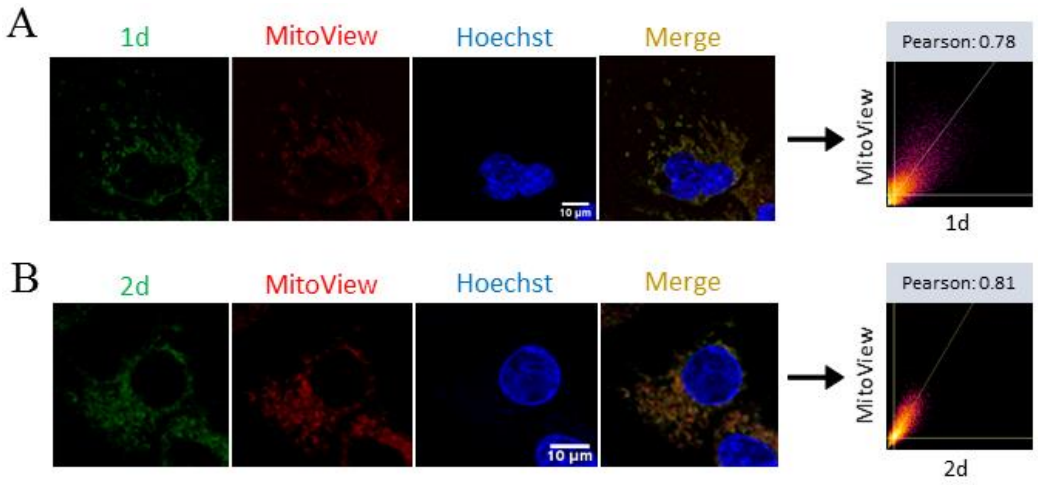

Figure 6. Assessment of fluorescence in cells co-stained with the mitochondrial dye MitoView. Nuclei were stained with Hoechst 33342 (blue), MitoView 633 (red) was then added and confocal fluorescence microscope images were obtained after 30-min-exposure to 1 µM **1d** (A) or 5 µM **2d** (B). Representative images and correlation between the green and the red fluorescent signal are displayed (Pearson´s coefficient).

To confirm the mitochondrial localization of the probes, cells were exposed to carbonyl cyanide m-chlorophenyl hydrazone (CCCP), a lipid-soluble weak acid and a potent mitochondrial uncoupling agent that causes acidification of the mitochondrial matrix, thus dissipating the transmembrane potential and depolarizing this organelle.[62] Incubation with CCCP, and then with pyrylium dyes, led to only residual staining of the mitochondria, both with **1d** and with **2d** (**Figure 7**). Considering the hydrophobic and cationic nature of the tested compounds, the observed location and the effect of CCCP, it can be concluded that pyrylium dyes **1c,d** and **2c,d** are electrostatically directed to mitochondria (likely accumulating in the mitochondrial membrane, a hydrophobic environment that enhances their emission and protect them against hydrolysis).

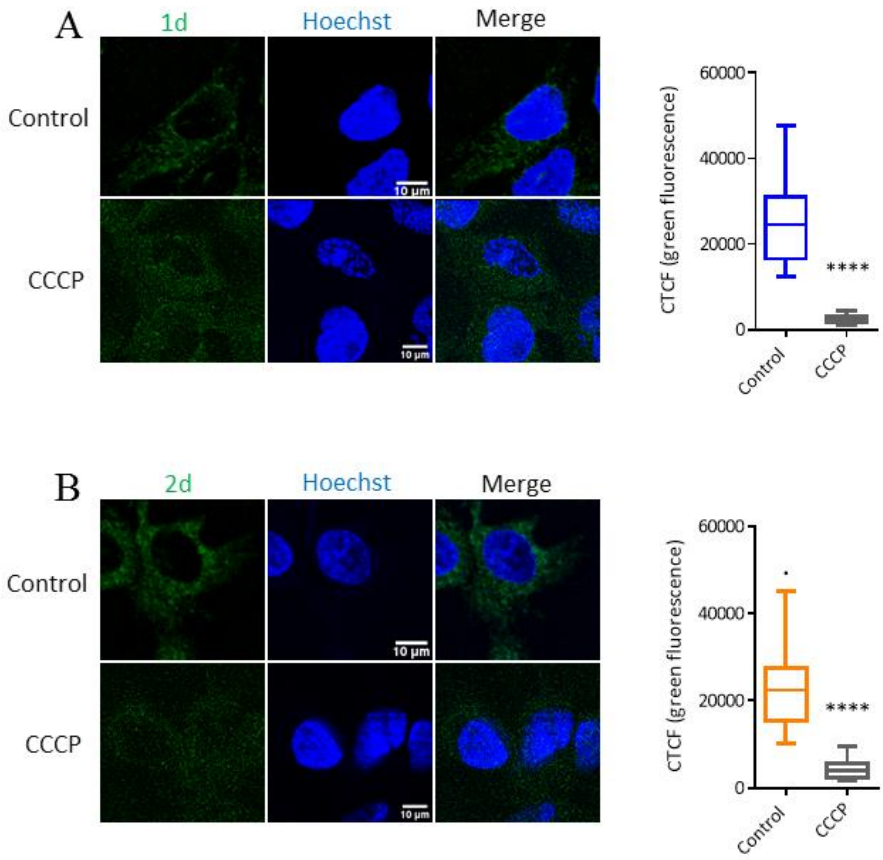

Figure 7. Assessment of fluorescence in cells treated with the mitochondrial membrane uncoupler CCCP. Cells were exposed to or not to CCCP (50 µM, 30 min). Nuclei were stained with Hoechst 33342 (blue) and confocal microscope images were obtained after 30-min-exposure to 1 µM **1d** (A) or 5 µM **2d** (B). Representative images and quantification of the green fluorescent signal (CTCF) are displayed. Data are shown as median ± IQR, n=3. Statistical analysis was performed by unpaired t-test (**** indicates a p-value ≤ 0.0001).

We next investigated the photostability of the probes compared to that of MitoView. This was achieved by performing time-lapse experiments exciting each probe with 4 consecutive laser lines at 100% laser intensity to induce loss of fluorescence signal. As shown in **Figure 8**, both **1d** and **2d** mitochondrial dyes decreased their CTFC values to around 60% while MitoView displayed a decrease to around 35% (**Figures 8A** and **8B**), after 10 minutes of irradiation. Slope values were calculated to obtain the speed of the signal decrease. We

found that both **1d** and **2d** possessed slower CTFC decrease (**Figure 8B**) when compared to MitoView, meaning a higher photostability.

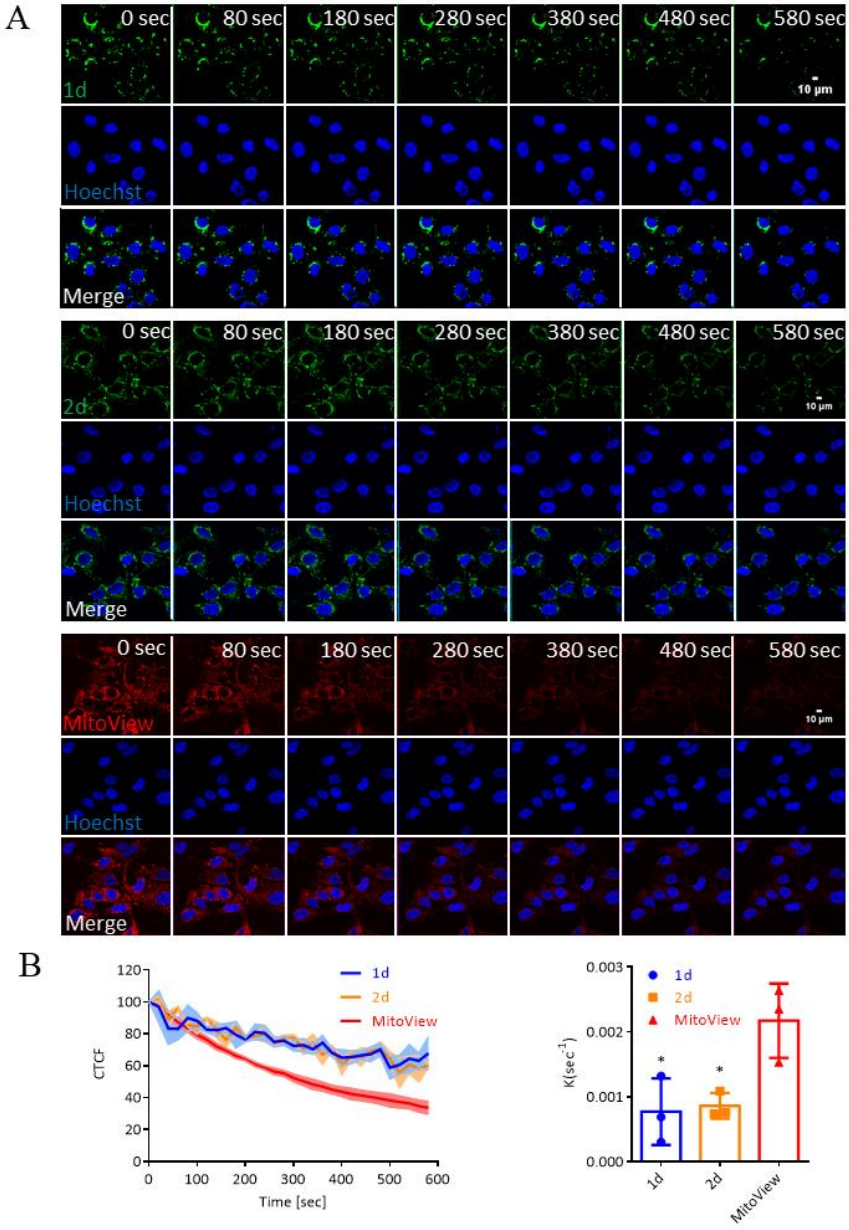

Figure 8. Analysis of the fluorescent probes photostability. Nuclei were stained with Hoechst 33342 (blue) and then 1µM of **1d**, 5µM of **2d** or 100 nM of MitoView was added. Time-lapse confocal microscopy images were taken every 20 sec for a total of 10 min. (A) Representative time-lapse images of the fluorescent signals of **1d**, **2d** and MitoView, respectively, (B) % of fluorescent signal quantifications (CTCF, corrected total cell fluorescence) are displayed for the 3 probes. The signal of each probe was normalised to the baseline at t=0. Slope values were calculated with one-phase decay

function in Graphpad Prism and expressed as K. Data are shown as mean ± SEM (standard error of the mean), n=3.

It is worth noting that the observed intracellular features demonstrate the potential utility of the studied probes for mitochondrial imaging. However more studies are needed to understand all the mechanistic details, since the presence of styryl moieties could make these probes susceptible to nucleophilic attack by biothiols (specially glutathione) and hence, the observed intracellular fluorescence could result from the corresponding adduct after reaction with the double bond (these details will be developed in future investigations).

Potential as anticancer drugs

Taking advantage of the efficient uptake by hepatocarcinoma cells of the four tested dyes, the possibility of using some of these compounds as anticancer drugs was also explored. In a classical and pioneering example, rhodamine 123 was first reported by the group of L. B. Chen as an efficient mitochondrial dye,[10] and later confirmed by the same group as a selective anticancer drug against pancreatic carcinoma line CRL 1420 and breast carcinoma line MCF-7.[63] In our case, toxicity assays were conducted to estimate at which order or magnitude molecules **1c,d** and **2c,d** showed promising activity in this regard against Hep3B cells. To assess the toxicity, acid phosphatase activity in culture was measured. Incubation of Hep3B cells with all the compounds (24 h - 0, 1, 3, 10, 30, 100, 300 μM) allowed to obtain the dose-response curves as shown in **Figure 9**. The following IC_{50} values were found: 4.2 μM (**2d**), 5.8 μM (**1d**), 6.5 μM (**2c**) and 11.5 μM (**1c**). These values are in line with the reported IC_{50} data for anticancer drugs against Hep3B cells. For instance, the IC_{50} of a series of drugs for Hep3B has been found in the micromolar range:[64] doxorubicin (4.5 μM), sorafenib (9.4 μM) and OSU-2S (2.8 μM). In another example with Hep3B cells, α-

mangostin was found to have an IC_{50} of 13.1 μM, whereas two derivatives of it have higher IC_{50} values (25 μM for Man-3DG and 12.5 for Man-6DG).[65] At the present stage it is not possible to point out to the mechanism explaining the toxicity of **1c,d** and **2c,d**, but considering the cationic and lipophilic nature of them, it may be suggested that the accumulation of dye in the mitochondria elicits mitochondrial-dependent cell death, as occurs for similar DLCs.[63] The fact that IC50 for these probes is relatively high after 24h treatment may be an obstacle in time-lapse imaging experiments in which live cells are maintained in presence of the dyes for longer periods, nevertheless such IC50 has no implication for short-incubation single-point imaging exemplified in the present paper with an incubation time of 30 min. The possibility of using pyrylium dyes as anticancer agents is well supported by the reported example of triarylpyrylium dye AA1, with an estimated IC_{50} of 6 μM against carcinoma cells CX-1[46] and even prolonging the survival of mice on *in vivo* assays. In that case, the inhibition of ATPase activity was found as the cause of the anticancer effect. The description of theranostic activities (imaging and antiproliferative) is not uncommon, as exemplifies the set of mitochondria-targeted F16 derivatives[5] or the family of isoquinolinum dyes[66] recently described.

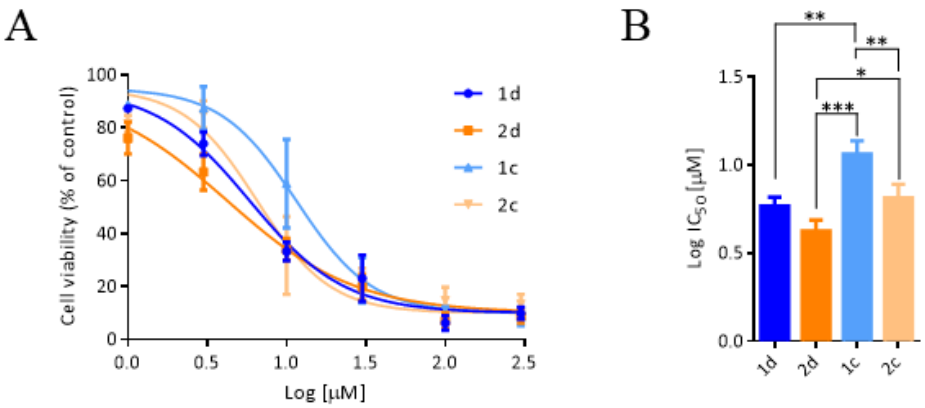

Figure 9. Assessment of cell viability after 24h-treatment with **1c**, **1d**, **2c** and **2d**. Cells were exposed to the mitochondrial probes in the concentration range (0, 1, 3, 10, 30, 100 and 300 μM). (A) Concentration-effect curves. (B) IC_{50} of each compound. Data are shown as mean ± SD, n=3. Statistical analysis was performed by one-way ANOVA followed by Tukey's multiple comparisons tests (* indicates a p-value ≤ 0.05, ** indicates a p-value ≤ 0.01 and *** indicates a p-value ≤ 0.001).

Conclusions

In summary, a family of eight styrylpyrylium dyes with different architectures (4 or 6-styryl) and substituents in the peripheral aromatic rings (R = -H, -CF_3, -OH and -OMe) have been synthesized and characterized both chemically ($^1H/^{13}C$ NMR, HRMS) and optically (UV-vis absorption and fluorescence steady-state / time-resolved spectroscopies). All the synthesized molecules have fluorescence in the yellow-orange range, and some of them display dual emission, arising from localized and delocalized excited states. The Stokes shift of six of the dyes exceeds 100 nm, reaching 193 nm in one case (**1d**). The biological studies have been carried out with the most stable dyes in an aqueous medium (**1c,d** and **2c,d**) using a human hepatoma cell line (Hep3B) and CLSM. It has been demonstrated that all the molecules stain mitochondria of Hep3B cells, through colocalization experiments (MitoView as reference probe) and by studying depolarization of the mitochondrial membrane with CCCP. Notably, the cytotoxic concentrations of the tested probes were found to be in the micromolar range (from 4.2 μM to 11.5 μM), similar to other know cytotoxic agents against this cancer cell line. Although the toxicity studies are preliminary, the dual activity of the presented dyes as imaging agents and potential anticancer molecules opens the way to further studies with optimized styrylpyrylium analogues as theranostic agents.

Conflicts of interest

There are no conflicts to declare.

Acknowledgements

F. G. acknowledges the support from Generalitat Valenciana (grant AICO/2020/322). I. M. R and F. L. thank Generalitat Valenciana for the economic support (Santiago Grisolía fellowship, ref. GRISOLIAP/2018/071 and postdoctoral contract, ref. APOSTD/2019/050, respectively).

Materials and methods

Reagents and instruments

All commercially available reagents and solvents were used as received. ^{1}H and ^{13}C NMR spectra were recorded at 25 °C with a 400 MHz Bruker Advance III HD spectrometer (101 MHz for ^{13}C-NMR). High-resolution mass spectra were obtained using a Waters Q-Tof Premier mass spectrometer with an electrospray source. UV-vis spectra were recorded using a 1 cm path length quartz cuvette on a Jasco V-630 UV-vis spectrophotometer. Steady-state emission was recorded with an Agilent Cary-Eclipse spectrofluorometer. Time-resolved fluorescence experiments were performed with an IBH5000U apparatus by using 464 nm (fwhm 1.4 ns) nanoLED as excitation source.

*Synthesis of compounds **1a-d***

Synthesis of 2,4-bis(4-methoxyphenyl)-6-methylpyrylium tetrafluoroborate

To a solution of *para*-methoxyacetophenone (6.5 g, 0.043 mol) in acetic anhydride (8.1 ml, 0.086 mol), BF_3 diethyl etherate (3.8 ml, 0.030 mol) was added dropwise under continuous stirring at room temperature. Then, the solution was heated to reflux at 138 °C for 2 hours. After cooling down to room temperature, the reaction mixture was poured into

200 ml of diethyl ether, and the red precipitate was recovered by filtration, washed with diethyl ether, and dried under vacuum (red solid, 3.0 g, yield 35 %).

^{1}H NMR (400 MHz, CD_3CN) δ 8.38 (d, *J* = 1.8 Hz, 1H), 8.29 – 8.24 (m, 2H), 8.22 – 8.17 (m, 2H), 7.93 (d, *J* = 1.8 Hz, 1H), 7.25 – 7.17 (m, 4H), 3.95 (s, 3H), 3.95 (s, 3H), 2.86 (s, 3H). ^{13}C NMR (101 MHz, CD_3CN) δ 175.30, 171.90, 167.20, 166.64, 164.66, 133.03, 131.73, 125.26, 122.20, 116.80, 116.54, 116.48, 113.02, 57.01, 56.94, 21.42. HRMS (ESI-TOF)$^+$ calculated for $C_{20}H_{19}O_3^+$ (M^+) (m/z): 307.1334; experimental (M^+) (m/z): 307.1334.

*Synthesis of styrylpyrylium dyes **1a-d***

To a suspension of 2,4-bis(4-methoxyphenyl)-6-methylpyrylium tetrafluoroborate (0.25 g, 0.64 mmol) in acetic acid (10 ml), the corresponding *para*-substituted aldehyde (5 or 10 equivalents), was added at room temperature. Then, the mixture was heated to reflux at 138 °C (a dark solution was formed) for 24 hours. After cooling down to room temperature, the crude reaction mixture was poured into 150 ml of diethyl ether, and the formed precipitate was recovered by filtration, washed with diethyl ether, and dried under vacuum before use.

1a. *(E)-2,4-bis(4-methoxyphenyl)-6-styrylpyrylium tetrafluoroborate* (red solid, 0.23 g, yield 75 %). ^{1}H NMR (400 MHz, CD_3CN) δ 8.28 – 8.23 (m, 2H), 8.20 (d, *J* = 1.8 Hz, 1H), 8.16 – 8.10 (m, 2H), 7.99 (d, *J* = 16.2 Hz, 1H), 7.95 (d, *J* = 1.7 Hz, 1H), 7.81 – 7.70 (m, 2H), 7.55 – 7.45 (m, 3H), 7.30 (d, *J* = 16.2 Hz, 1H), 7.18 – 7.12 (m, 4H), 3.92 (s, 3H), 3.92 (s, 3H). ^{13}C NMR (101 MHz, CD_3CN) δ 169.76, 168.32, 166.97, 166.48, 163.18, 144.94, 135.29, 132.80, 132.69, 131.76, 130.30, 129.86, 125.24, 122.05, 118.82, 116.64, 116.42, 115.32, 112.21, 56.89, 56.81. HRMS (ESI-TOF)$^+$ calculated for $C_{27}H_{23}O_3^+$ (M^+) (m/z): 395.1647; experimental (M^+) (m/z): 395.1645.

1b. *(E)-2,4-bis(4-methoxyphenyl)-6-(4-(trifluoromethyl)styryl)pyrylium tetrafluoroborate* (orange solid, 0.29 g, yield 84 %). ^{1}H NMR (400 MHz, CD_3CN) δ 8.41 – 8.34 (m, 3H), 8.26 – 8.20 (m, 2H), 8.14 (d, *J* = 16.3 Hz, 1H), 8.10 (d, *J* = 1.7 Hz, 1H), 7.98 (d, *J* = 8.4 Hz, 2H), 7.84 (d, *J* = 8.3 Hz, 2H), 7.49 (d, *J* = 16.3 Hz, 1H), 7.28 – 7.21 (m, 4H), 3.98 (s, 3H), 3.97 (s, 3H). ^{13}C NMR (101 MHz, CD_3CN) δ 170.26, 167.24, 166.81, 166.39, 163.53, 142.11, 132.49, 131.72, 129.76, 126.75, 125.08, 121.86, 121.21, 116.41, 116.15, 115.85, 112.97, 56.61, 56.56. HRMS (ESI-TOF)$^+$ calculated for $C_{28}H_{22}F_3O_3^+$ (M^+) (m/z): 463.1521; experimental (M^+) (m/z): 463.1514.

1c. *(E)-2-(4-hydroxystyryl)-4,6-bis(4-methoxyphenyl)pyrylium tetrafluoroborate* (dark brown solid, 0.27 g, yield 87 %). ^{1}H NMR (400 MHz, CD_3CN) δ 8.33 – 8.29 (m, 2H), 8.23 (d, *J* = 1.7 Hz, 1H), 8.21 – 8.14 (m, 2H), 8.09 (d, *J* = 16.1 Hz, 1H), 7.96 (d, *J* = 1.6 Hz, 1H), 7.73 (d, *J* = 8.7 Hz, 2H), 7.25 – 7.18 (m, 5H), 6.97 (d, *J* = 8.7 Hz, 2H), 3.96 (s, 3H), 3.96 (s, 3H). ^{13}C NMR (101 MHz, CD_3CN) δ 169.23, 168.97, 166.29, 165.84, 162.55, 161.64, 145.49, 132.11, 132.06, 131.17, 127.15, 125.34, 122.10, 117.01, 116.23, 115.99, 115.38, 114.66, 111.57, 56.50, 56.45. HRMS (ESI-TOF)$^+$ calculated for $C_{27}H_{23}O_4^+$ (M^+) (m/z): 411.1596; experimental (M^+) (m/z): 411.1594.

1d. *(E)-2,4-bis(4-methoxyphenyl)-6-(4-methoxystyryl)pyrylium tetrafluoroborate* (brown solid, 0.24 g, yield 74 %). ^{1}H NMR (400 MHz, DMSO-d_6) δ 8.67 (d, *J* = 1.5 Hz, 1H), 8.54 – 8.46 (m, 2H), 8.45 – 8.37 (m, 3H), 8.22 (d, *J* = 16.2 Hz, 1H), 7.85 (d, *J* = 8.8 Hz, 2H), 7.44 (d, *J* = 16.2 Hz, 1H), 7.29 – 7.21 (m, 4H), 7.12 (d, *J* = 8.9 Hz, 2H), 3.95 (s, 3H), 3.94 (s, 3H), 3.87 (s, 3H). ^{13}C NMR (101 MHz, DMSO-d_6) δ 168.27, 167.72, 165.10, 164.50, 162.44, 161.00, 143.93, 131.88, 131.14, 130.80, 127.23, 124.55, 121.54, 116.05, 115.51, 115.25,

115.00, 113.70, 56.11, 56.01, 55.63. HRMS (ESI-TOF)$^+$ calculated for $C_{28}H_{25}O_4^+$ (M^+) (m/z): 425.1753; experimental (M^+) (m/z): 425.1747.

*Synthesis of compounds **2a-d***

Synthesis of 2,6-bis(4-methoxyphenyl)-4-methylpyrylium tetrafluoroborate

2,6-bis(4-methoxyphenyl)pyrylium hydrogen sulfate (orange solid, 2.4 g, yield 28 %). To a solution of *para*-methoxyacetophenone (6.5 g, 0.043 mol) in triethyl orthoformate (14.4 ml, 0.086 mol), H_2SO_4 (1.2 ml, 0.020 mol) was added dropwise under continuous stirring at room temperature. Then, the solution was heated to reflux at 100 °C for 2 hours. After cooling down to room temperature, the reaction mixture was poured into 200 ml of ethyl acetate, and the orange precipitate was recovered by filtration, washed with ethyl acetate, and dried under vacuum.

^{1}H NMR (400 MHz, CD_3CN) δ 8.68 (t, *J* = 8.4 Hz, 1H), 8.34 – 8.27 (m, 4H), 8.21 (d, *J* = 8.4 Hz, 2H), 7.32 – 7.23 (m, 4H), 4.01 (s, 6H). ^{13}C NMR (101 MHz, CD_3CN) δ 171.85, 166.95, 155.61, 132.04, 121.85, 117.55, 116.76, 56.96. HRMS (ESI-TOF)$^+$ calculated for $C_{19}H_{17}O_3^+$ (M^+) (m/z): 293.1178; experimental (M^+) (m/z): 293.1171.

2,6-bis(4-methoxyphenyl)-4-methyl-4H-pyran (brown oil, 1.65 g, quantitative). To a suspension of *2,6-bis(4-methoxyphenyl)pyrylium hydrogen sulfate* (2.1 g, 5.4 mmol) in anhydrous diethyl ether (50 ml), 3 M solution of CH_3MgI in diethyl ether (26.9 ml, 80.7 mmol) was added dropwise under nitrogen atmosphere. Then, the mixture was allowed to react overnight under continuous stirring at room temperature. After that, the crude reaction mixture was poured into 20 ml of distilled water and extracted 3 x 40 ml with NH_4Cl (ss) and

3 x 40 ml with water. The organic phase was dried over Na_2SO_4 and the solvent was evaporated under vacuum, to give a dark sticky residue, used without purification.

^{1}H NMR (400 MHz, CD_3CN) δ 7.65 – 7.60 (m, 4H), 6.97 – 6.93 (m, 4H), 5.36 (d, *J* = 3.7 Hz, 2H), 3.81 (s, 6H), 3.22 – 3.13 (m, 1H), 1.21 (d, *J* = 6.8 Hz, 3H). ^{13}C NMR (101 MHz, CD_3CN) δ 160.83, 148.48, 129.06, 128.09, 126.64, 119.21, 118.26, 114.93, 114.72, 101.93, 55.96, 27.53, 25.20.

2,6-bis(4-methoxyphenyl)-4-methylpyrylium tetrafluoroborate (light brown solid, 0.95 g, yield 45 %). To a solution of *2,6-bis(4-methoxyphenyl)-4-methyl-4H-pyran* (1.65 g, 5.4 mmol) in anhydrous acetonitrile (50 ml), Ph_3CBF_4 (1.95 g, 5.9 mmol) was added under nitrogen atmosphere. Then, the mixture was allowed to react for 3 hours under continuous stirring at room temperature. After that, the solvent was evaporated under vacuum and the residue was dissolved in the minimum volume of acetone and poured into 200 ml of ethyl acetate. The brown precipitate was recovered by filtration, washed with ethyl acetate, and dried under vacuum.

^{1}H NMR (400 MHz, CD_3CN) δ 8.26 – 8.21 (m, 4H), 8.09 (d, *J* = 0.5 Hz, 2H), 7.26 – 7.21 (m, 4H), 3.96 (s, 6H), 2.72 (s, 3H). ^{13}C NMR (101 MHz, CD_3CN) δ 171.91, 170.03, 166.55, 131.68, 121.75, 118.36, 116.64, 56.88, 23.78. HRMS (ESI-TOF)$^+$ calculated for $C_{20}H_{19}O_3^+$ (M^+) (m/z): 307.1334; experimental (M^+) (m/z): 307.1332.

Synthesis of styrylpyrylium dyes ***2a-d***

To a suspension of *2,6-bis(4-methoxyphenyl)-4-methylpyrylium tetrafluoroborate* (0.25 g, 0.64 mmol) in acetic acid (10 ml), the correspondent *para*-substituted aldehyde (5 or 10 equivalents), was added at room temperature. Then, the mixture was heated to reflux

at 138 °C (a dark solution was formed) for 24 hours. After cooling down to room temperature, the reaction mixture was poured into 150 ml of diethyl ether, and the formed precipitate was recovered by filtration, washed with diethyl ether, and dried under vacuum before use.

2a. *(E)-2,6-bis(4-methoxyphenyl)-4-styrylpyrylium tetrafluoroborate* (brown solid, 0.19 g, yield 63 %). ^{1}H NMR (400 MHz, CD_3CN) δ 8.26 – 8.17 (m, 5H), 8.15 (s, 2H), 7.84 – 7.74 (m, 2H), 7.59 – 7.49 (m, 3H), 7.38 (d, *J* = 16.2 Hz, 1H), 7.24 – 7.16 (m, 4H), 3.94 (s, 6H). ^{13}C NMR (101 MHz, CD_3CN) δ 169.54, 166.32, 162.63, 148.26, 135.68, 133.24, 131.36, 130.45, 130.21, 124.01, 122.20, 116.56, 113.17, 56.83. HRMS (ESI-TOF)$^+$ calculated for $C_{27}H_{23}O_3^+$ (M^+) (m/z): 395.1647; experimental (M^+) (m/z): 395.1645.

2b. *(E)-2,6-bis(4-methoxyphenyl)-4-(4-(trifluoromethyl)styryl)pyrylium tetrafluoroborate* (brown solid, 0.30 g, yield 86%). ^{1}H NMR (300 MHz, CD_3CN) δ 8.31 – 8.15 (m, 7H), 7.93 (d, *J* = 8.3 Hz, 2H), 7.82 (d, *J* = 8.3 Hz, 2H), 7.48 (d, *J* = 16.3 Hz, 1H), 7.26 – 7.18 (m, 4H), 3.95 (s, 6H). ^{13}C NMR (75 MHz, CD_3CN) δ 169.79, 166.11, 145.09, 131.16, 129.98, 126.85, 126.79, 121.82, 116.24, 113.39, 56.50. HRMS (ESI-TOF)$^+$ calculated for $C_{28}H_{22}F_3O_3^+$ (M^+) (m/z): 463.1521; experimental (M^+) (m/z): 463.1515.

2c. *(E)-4-(4-hydroxystyryl)-2,6-bis(4-methoxyphenyl)pyrylium tetrafluoroborate* (brown solid, 0.22 g, yield 71 %). ^{1}H NMR (400 MHz, DMSO-d_6) δ 10.68 (s, 1H), 8.50 – 8.41 (m, 3H), 8.30 – 8.23 (m, 4H), 7.68 (d, *J* = 8.8 Hz, 2H), 7.27 (d, *J* = 16.1 Hz, 1H), 7.26 – 7.20 (m, 4H), 6.96 (d, *J* = 8.7 Hz, 2H), 3.92 (s, 6H). ^{13}C NMR (101 MHz, DMSO-d_6) δ 166.90, 164.27, 162.25, 161.54, 148.43, 132.03, 130.14, 126.22, 121.61, 120.11, 116.76, 115.44, 111.56, 56.00. HRMS (ESI-TOF)$^+$ calculated for $C_{27}H_{23}O_4^+$ (M^+) (m/z): 411.1596; experimental (M^+) (m/z): 411.1599.

2d. *(E)-2,6-bis(4-methoxyphenyl)-4-(4-methoxystyryl)pyrylium tetrafluoroborate* (dark red solid, 0.19 g, yield 58 %). ^{1}H NMR (400 MHz, CD_3CN) δ 8.24 – 8.16 (m, 5H), 8.06 (s, 2H), 7.79 – 7.72 (m, 2H), 7.26 – 7.17 (m, 5H), 7.10 – 7.03 (m, 2H), 3.95 (s, 6H), 3.89 (s, 3H). ^{13}C NMR (101 MHz, CD_3CN) δ 168.67, 165.90, 164.46, 162.57, 148.71, 132.56, 130.96, 128.35, 122.22, 121.29, 116.30, 115.94, 112.31, 56.63, 56.33. HRMS (ESI-TOF)$^+$ calculated for $C_{28}H_{25}O_4^+$ (M^+) (m/z): 425.1753; experimental (M^+) (m/z): 425.1747.

Photophysical characterization of the compounds

1 mM stock solutions of compounds **1a-d** and **2a-d** were prepared in acetonitrile (in dimethyl sulfoxide for compound **1d**). For UV-vis spectra measurements, the corresponding stock solution for each compound was diluted to reach a final concentration of 10 µM, in dichloromethane (DMC), acetonitrile (ACN) and phosphate-buffered saline (PBS, 10 mM, pH 7.4). For fluorescence spectra acquisition, concentration was adjusted to reach a value of 0.1 in absorbance, to minimize the primary inner filter effect. λ_{exc} was set at the absorption maximum of each compound.

Fluorescence Quantum Yield Measurements (ϕ_F). The fluorescence quantum yields of all compounds were determined in DCM, ACN, and PBS (10 mM, pH 7.4), under an N_2 atmosphere. *(E)-2-(4-methoxystyryl)-4,6-diphenylpyrylium tetrafluoroborate* was used as a reference since its fluorescence quantum yield was described in DCM (ϕ_F = 0.38).[49,53]

The concentration of the reference and the studied compounds were adjusted to obtain the same absorption at the excitation wavelength. Fluorescence quantum yields were calculated by using [Equation (1)]:

$$\phi_F = \phi_R \cdot (A_R \cdot F_S / A_S \cdot F_R) \cdot (n_S^2 / n_R^2) \qquad (1)$$

where ϕ_F is the fluorescence quantum yield, F is the integral of the emission spectrum, A is the absorption intensity, and n is the refractive index. The sub-index R refers to the reference compound and S to the studied pyrylium salt.

Fluorescence Lifetime Measurements (τ_F). The fluorescence lifetimes of all compounds were determined in DCM, ACN, and PBS (10 mM, pH 7.4) under an N_2 atmosphere. Solutions were prepared similarly to those used to obtain the emission spectra. Fluorescence lifetimes were determined by using the technique of time-correlated single-photon counting (TCSPC). Data obtained from the experiments were adjusted to a single or double exponential model by using the software IBH DAS6.

Cell culture and treatments

Hep3B (ATCC HB-8064), a human hepatoblastoma cell line was employed to test the fluorescent dyes in an *in vitro* setting. Cell cultures were maintained in MEM supplemented with 10 % inactivated fetal bovine serum, 2 mM L-glutamine, non-essential amino acids, and 1 mM sodium pyruvate at 37^0C, in a cell culture incubator (MCO-19AICUV-PE, Panasonic Healthcare Co. Ltd., Tokyo, Japan) with a humidified 5 % CO_2/95 % air atmosphere (AirLiquide Medical, Valencia, Spain). Cell cultures were maintained in the presence of penicillin (50 units/mL) and streptomycin (50 μg/mL) and used for experiments at a passage number lower than 25. Reagents employed in cell culture were purchased from ThermoFisher Scientific (Walthman, MA, USA).

Cell viability assay

Cell viability was assessed by means of acid phosphatase assay, based on the conversion of *p*-NPP to *para*-nitrophenol by cytosolic acid phosphatase.[67] Cells were seeded

in a 96-well-plate ($15x10^4$ cells/well) and treated with increasing concentrations of the mitochondrial fluorescent dyes (1, 3, 10, 30, 100 and 300 μM) in complete cell culture medium. After 24 h, the medium was removed and each well was washed once with 100 μl PBS, 100 μl of assay buffer (0.1 M sodium acetate at pH 5.0, 0.1% Triton X-100), and 7.25 mM *p*-NNP was then added. Plates were incubated at 37°C for 2 h. The reaction was stopped with the addition of 50 μl of 1 M NaOH and color development was evaluated at 405 nm using a Multiskan® EX plate reader (ThermoFisher Scientific). The non-enzymatic hydrolysis of the pNPP substrate was determined by including wells that contained the assay solution without cells.

Live cell imaging

Hep3B cell line was obtained from the American Type Culture Collection (ATCC, Manassas, VA, USA). Cells were seeded (15×10^4/well) in sterile μ-Slide 8-well-chamber slide (Ibidi, Inycom, Madrid, Spain) and let to adhere overnight. The next day, cells were incubated with 0.5, 1 or 5 μM of the mitochondrial fluorescent dyes in Krebs-HEPES buffer (140 mM NaCl, 5.9 mM KCl, 1.2 mM $MgCl_2$, 15 mM HEPES) supplemented with 2.5 mM $CaCl_2$, and 5 mM D-glucose. 100 nM Hoechst 33342 (Merck KGaA, Darmstadt, Germany) was added to stain nuclei. In some experiments, 100 nM MitoView™ 633 (Biotyum, Hayward, CA, USA) was also added - a far-red fluorescent mitochondrial dye with absorbance/emission at 622/648 nm. For treatment with CCCP (carbonyl cyanide m-chlorophenyl hydrazone), a protonophore that uncouples the proton gradient established by the electron transport chain,[68] cells were treated with 50 μM of this compound for 30 minutes before staining with the mitochondrial probes. The plate was then transferred to a heated stage above a 40x magnification with HCxPL APO CS2 40.0 x 1.30 oil UV objective on an

inverted confocal laser-scanning microscope (Leica DMI8-CS) equipped with a white light laser and a diode laser. Measurements were carried out using excitation at 488 nm with a pixel dwell time of 1.5 μs; two to three FOV (field of view) were recorded for each condition/probe. The detection range was set to 500-625 nm for the mitochondrial dyes, with pinholes set to 1 Airy unit.

For the photostability experiments, cells were incubated with 1 μM **1d**, 5μM **2d** or 100 nM MitoView™ 633 in full medium (with Hoechst to mark nuclei). The plate was then transferred to a heated stage (37°C) above a 40x magnification with HCxPL APO CS2 40.0 x 1.30 oil UV objective on an inverted confocal laser-scanning microscope (Leica TCS-SP8) as before. To induce loss of fluorescence signal, all dyes were illuminated with their respective wavelength using 4 lines of laser set up to 100% power. Time-lapse images were taken every 20 seconds for a total of 10 minutes.

Image processing and analysis

Images were processed with ImageJ2 (National Institutes of Health, Bethesda, MD, USA); a subtract background function was employed with a sliding paraboloid function of 50 pixels followed by a median filtering function used with a radius of 1 pixel. Single cells were selected with the ROI manager using the polygon selection and the area of selected cells, the mean fluorescence and the integrated density measured. Corrected total cell fluorescence (CTCF) was calculated by subtracting the integrated density to the product of the area and mean fluorescence of the background. For colocalization, we employed the colocalization threshold plugin in ImageJ2. Data were then represented using Graphpad Prism.

For the photostability analysis, images were processed as before. Individual cells were marked in the ROI manager of ImageJ2 and the multi-measure function was employed to obtain the above-mentioned values across the time-lapse experiment. CTFC values were calculated as before and normalized considering the values at time 0. From the CTFC time-lapse curves, the K values (the slope of the curves) were obtained using a one-phase decay function in GraphPad Prism.

References

1 C. Ma, F. Xia and S. O. Kelley, *Bioconjug. Chem.*, 2020, **31**, 2650–2667.

2 S. Samanta, Y. He, A. Sharma, J. Kim, W. Pan, Z. Yang, J. Li, W. Yan, L. Liu, J. Qu and J. S. Kim, *Chem*, 2019, **5**, 1697–1726.

3 J. S. Modica-Napolitano and J. R. Aprille, *Adv. Drug Deliv. Rev.*, 2001, **49**, 63–70.

4 J. Zielonka, J. Joseph, A. Sikora, M. Hardy, O. Ouari, J. Vasquez-Vivar, G. Cheng, M. Lopez and B. Kalyanaraman, *Chem. Rev.*, 2017, **117**, 10043–10120.

5 H. Chen, J. Wang, X. Feng, M. Zhu, S. Hoffmann, A. Hsu, K. Qian, D. Huang, F. Zhao, W. Liu, H. Zhang and Z. Cheng, *Chem. Sci.*, 2019, **10**, 7946–7951.

6 W. Xu, Z. Zeng, J. H. Jiang, Y. T. Chang and L. Yuan, *Angew. Chemie - Int. Ed.*, 2016, **55**, 13658–13699.

7 M. C. Harwig, M. P. Viana, J. M. Egner, J. J. Harwig, M. E. Widlansky, S. M. Rafelski and R. B. Hill, *Anal. Biochem.*, 2018, **552**, 81–99.

8 P. Gao, W. Pan, N. Li and B. Tang, *Chem. Sci.*, 2019, **10**, 6035–6071.

9 K. Yu, J. Pan, E. Husamelden, H. Zhang, Q. He, Y. Wei and M. Tian, *Chem. - An Asian J.*, 2020, **15**, 3942–3960.

10 L. V. Johnson, M. L. Walsh and L. B. Chen, *Proc. Natl. Acad. Sci. U. S. A.*, 1980, **77**, 990–994.

11 H. He, Z. Ye, Y. Xiao, W. Yang, X. Qian and Y. Yang, *Anal. Chem.*, 2018, **90**, 2164–2169.

12 X. Zhou, Y. Fang, L. Lesiak and C. I. Stains, *ChemBioChem*, 2019, **20**, 1712–1716.

13 M. I. Sánchez, J. Martínez-Costas, J. L. Mascareñas and M. E. Vázquez, *ACS Chem. Biol.*, 2014, **9**, 2742–2747.

14 M. I. Sánchez, Y. Vida, E. Pérez-Inestrosa, J. L. Mascareñas, M. E. Vázquez, A. Sugiura and J. Martínez-Costas, *Sci. Rep.*, 2020, **10**, 1–12.

15 A. Gandioso, R. Bresolí-Obach, A. Nin-Hill, M. Bosch, M. Palau, A. Galindo, S. Contreras, A. Rovira, C. Rovira, S. Nonell and V. Marchán, *J. Org. Chem.*, 2018, **83**, 1185–1195.

16 A. Gandioso, M. Palau, R. Bresolí-Obach, A. Galindo, A. Rovira, M. Bosch, S. Nonell and V. Marchán, *J. Org. Chem.*, 2018, **83**, 11519–11531.

17 A. Rovira, M. Pujals, A. Gandioso, M. López-Corrales, M. Bosch and V. Marchán, *J. Org. Chem.*, 2020, **85**, 6086–6097.

18 N. Jiang, J. Fan, F. Xu, X. Peng, H. Mu, J. Wang and X. Xiong, *Angew. Chemie*, 2015, **127**, 2540–2544.

19 H. Wang, J. Hu, G. Yang, X. Zhang, R. Zhang, K. Uvdal, Z. Zhang, X. Wu and Z. Hu, *Sensors Actuators, B Chem.*, 2020, **320**, 128418.

20 L. Krčová, S. Rimpelová, M. Havlík, B. Dolenský, F. Vellieux, T. Ruml, P. Martásek, V. Král and T. Bříza, *Dye. Pigment.*, 2020, **172**, 107802.

21 E. Hase, H. Takanari, K. Hoshi, M. Okamoto, A. Tabata, H. Nagamune, T. Minamikawa, T. Yasui, Y. Yoshida, K. Minagawa, Y. Kawamura, Y. Imada and F. Yagishita, *Org. Biomol. Chem.*, 2020, **18**, 7571–7576.

22 J. Yang, R. Zhang, Y. Zhao, J. Tian, S. Wang, C. P. Gros and H. Xu, *Spectrochim. Acta - Part A Mol. Biomol. Spectrosc.*, 2021, **248**, 119199.

23 C. W. T. Leung, Y. Hong, S. Chen, E. Zhao, J. W. Y. Lam and B. Z. Tang, *J. Am. Chem. Soc.*, 2013, **135**, 62–65.

24 J. Li, N. Kwon, Y. Jeong, S. Lee, G. Kim and J. Yoon, *ACS Appl. Mater. Interfaces*, 2018, **10**, 12150–12154.

25 Z. Yang, L. Li, J. Ling, T. Liu, X. Huang, Y. Ying, Y. Zhao, Y. Zhao, K. Lei, L. Chen and Z. Chen, *Chem. Sci.*, 2020, **11**, 8506–8516.

26 X. Mu, Y. Liu, S. Liu, Y. Sun, N. Lu, Y. Lu, W. Li, X. Zhou, B. Liu and Z. Li, *Sensors Actuators, B Chem.*, 2019, **298**, 126831.

27 P. Herrero-Foncubierta, M. del C. González-García, S. Resa, J. M. Paredes, C. Ripoll, M. D. Girón, R. Salto, J. M. Cuerva, A. Orte and D. Miguel, *Dye. Pigment.*, 2020, **183**, 108649.

28 A. Blázquez-Moraleja, I. Sáenz-De-Santa María, M. D. Chiara, D. Álvarez-Fernández, I. García-Moreno, R. Prieto-Montero, V. Martínez-Martínez, I. López Arbeloa and J. L. Chiara, *Chem. Sci.*, 2020, **11**, 1052–1065.

29 M. P. Murphy and R. C. Hartley, *Nat. Rev. Drug Discov.*, 2018, **17**, 865–886.

30 Y. Yamada, Satrialdi, M. Hibino, D. Sasaki, J. Abe and H. Harashima, *Adv. Drug Deliv. Rev.*, 2020, **154**–**155**, 187–209.

31 P. L. Toogood, *Curr. Opin. Chem. Biol.*, 2008, **12**, 457–463.

32 M. A. Miranda and H. García, *Chem. Rev.*, 1994, **94**, 1063–1089.

33 M. A. Miranda, M. A. Izquierdo and F. Galindo, *Org. Lett.*, 2001, **3**, 1965–1966.

34 N. A. Romero and D. A. Nicewicz, *Chem. Rev.*, 2016, **116**, 10075–10166.

35 F. Galindo and M. A. Miranda, *J. Photochem. Photobiol. A Chem.*, 1998, **113**, 155–161.

36 T. Y. Ohulchanskyy, M. K. Gannon, Y. Mao, A. Skripchenko, S. J. Wagner, P. N. Prasad and M. R. Detty, *J. Phys. Chem. B*, 2007, **111**, 9686–9692.

37 D. Jiménez, R. Martínez-Máñez, F. Sancenón, J. V. Ros-Lis, A. Benito and J. Soto, *J. Am. Chem. Soc.*, 2003, **125**, 9000–9001.

38 A. Beltrán, M. I. Burguete, F. Galindo and S. V. Luis, *New J. Chem.*, 2020, **44**, 9509–

9521.

39 D. Moser, Y. Duan, F. Wang, Y. Ma, M. J. O'Neill and J. Cornella, *Angew. Chemie - Int. Ed.*, 2018, **57**, 11035–11039.

40 I. Muñoz Resta, J. F. Miravet, M. Yamaji and F. Galindo, *J. Mater. Chem. C*, 2020, **8**, 14348–14352.

41 S. Chakraborty, M. M. Joseph, S. Varughese, S. Ghosh, K. K. Maiti, A. Samanta and A. Ajayaghosh, *Chem. Sci.*, 2020, 12695–12700.

42 A. Beltrán, M. Isabel Burguete, D. R. Abánades, D. Pérez-Sala, S. V. Luis and F. Galindo, *Chem. Commun.*, 2014, **50**, 3579–3581.

43 E. Molnár, S. Kuntam, P. K. R. Cingaram, B. Peksel, B. Suresh, G. Fábián, L. Z. Fehér, A. Bokros, Á. Medgyesi, F. Ayaydin and L. G. Puskás, *Molecules*, 2013, **18**, 9999–10013.

44 S. Y. Wen, W. Zhang, T. B. Ren, Q. L. Zhang, Y. P. Liu, L. Shi, R. Hu, X. B. Zhang and L. Yuan, *Chem. - A Eur. J.*, 2019, **25**, 6973–6979.

45 X. Chen, L. Yan, Y. Liu, Y. Yang and J. You, *Chem. Commun.*, 2020, 15080–15083.

46 X. Sun, K. Song, J. Hu and K. D. Garlid, *Cancer Res.*, 1994, **54**, 1465–1471.

47 N. K. Brennan, J. P. Hall, S. R. Davies, S. O. Gollnick, A. R. Oseroff, S. L. Gibson, R. Hilf and M. R. Detty, *J. Med. Chem.*, 2002, **45**, 5123–5135.

48 A. Dinculescu, T. S. Balaban, C. Popescu, D. Toader and A. T. Balaban, *Bull. des Sociétés Chim. Belges*, 1991, **100**, 665–672.

49 F. Haucke, Gunter; Czerney, Peter; Cebulla, *Berichte der Bunsengesellschaft für Phys. Chemie*, 1992, **96**, 880–886.

50 L. D. Lavis, *Biochemistry*, 2017, **56**, 5165–5170.

51 D. Wu, A. C. Sedgwick, T. Gunnlaugsson, E. U. Akkaya, J. Yoon and T. D. James,

Chem. Soc. Rev., 2017, **46**, 7105–7123.

52 Y. Fu and N. S. Finney, *RSC Adv.*, 2018, **8**, 29051–29061.

53 A. Beltrán, M. I. Burguete, S. V. Luis and F. Galindo, *European J. Org. Chem.*, 2017, 4864–4870.

54 S. Elsayed, A. Agostini, L. E. Santos-Figueroa, R. Martínez-Máñez and F. Sancenón, *ChemistryOpen*, 2013, **2**, 58–62.

55 P. Nikolov and S. Metzov, *J. Photochem. Photobiol. A Chem.*, 2000, **135**, 13–25.

56 A. Pigliucci, P. Nikolov, A. Rehaman, L. Gagliardi, C. J. Cramer and E. Vauthey, *J. Phys. Chem. A*, 2006, **110**, 9988–9994.

57 F. Pina, M. J. Melo, C. A. T. Laia, A. J. Parola and J. C. Lima, *Chem. Soc. Rev.*, 2012, **41**, 869–908.

58 T. B. Ren, W. Xu, W. Zhang, X. X. Zhang, Z. Y. Wang, Z. Xiang, L. Yuan and X. B. Zhang, *J. Am. Chem. Soc.*, 2018, **140**, 7716–7722.

59 A. V. Saura, M. J. Marín, M. I. Burguete, D. A. Russell, F. Galindo and S. V. Luis, *Org. Biomol. Chem.*, 2015, **13**, 7736–7749.

60 A. Vanessa Saura, M. Isabel Burguete, F. Galindo and S. V. Luis, *Org. Biomol. Chem.*, 2017, **15**, 3013–3024.

61 C. W. Hsieh, C. H. Chu, H. M. Lee and W. Yuan Yang, *Sci. Rep.*, 2015, **5**, 1–13.

62 P. G. Heytler and W. W. Prichard, *Biochem. Biophys. Res. Commun.*, 1962, **7**, 272–275.

63 T. J. Lampidis, S. D. Bernal, I. C. Summerhayes and L. B. Chen, *Cancer Res.*, 1983, **43**, 716–720.

64 H. A. Omar, D. M. Zaher, V. Srinivasulu, F. Hersi, H. Tarazi and T. H. Al-Tel, *Eur. J. Med. Chem.*, 2017, **139**, 804–814.

65 S. M. Kim, J. M. Han, T. T. Le, J. K. Sohng and H. J. Jung, *Int. J. Mol. Sci.*, 2020, **21**, 1–19.

66 M. Y. Wu, L. Liu, Q. Zou, J. K. Leung, J. L. Wang, T. Y. Chou and S. Feng, *J. Mater. Chem. B*, 2020, **8**, 9035–9042.

67 T. T. Yang, P. Sinai and S. R. Kain, *Anal. Biochem.*, 1996, **241**, 103–108.

68 E. Gottlieb, S. M. Armour, M. H. Harris and C. B. Thompson, *Cell Death Differ.*, 2003, **10**, 709–717.